Published in final edited form as:
Acta Neuropathol. 2015 February ; 129(2): 221–237. doi:10.1007/s00401-014-1373-0.

Differential induction and spread of tau pathology in young PS19 tau transgenic mice following intracerebral injections of pathological tau from Alzheimer's disease or corticobasal degeneration brains

Susana Boluda, **Michiyo Iba**, **Bin Zhang**, **Kevin M. Raible**, **Virginia M-Y. Lee**, and **John Q. Trojanowski**

Department of Pathology and Laboratory Medicine, The Center for Neurodegenerative Disease Research, Institute on Aging, University of Pennsylvania, Perelman School of Medicine, 3600 Spruce Street, Philadelphia, PA 19104-4283, USA

Abstract

Filamentous tau pathologies are hallmark lesions of several neurodegenerative tauopathies including Alzheimer's disease (AD) and corticobasal degeneration (CBD) which show cell type-specific and topographically distinct tau inclusions. Growing evidence supports templated transmission of tauopathies through functionally interconnected neuroanatomical pathways suggesting that different self-propagating strains of pathological tau could account for the diverse manifestations of neurodegenerative tauopathies. Here, we describe the rapid and distinct cell type-specific spread of pathological tau following intracerebral injections of CBD or AD brain extracts enriched in pathological tau (designated CBD-Tau and AD-Tau, respectively) in young human mutant P301S tau transgenic (Tg) mice (line PS19) ~6–9 months before they show onset of mutant tau transgene-induced tau pathology. At 1 month post-injection of CBD-Tau, tau inclusions developed predominantly in oligodendrocytes of the fimbria and white matter near the injection sites with infrequent intraneuronal tau aggregates. In contrast, injections of AD-Tau in young PS19 mice induced tau pathology predominantly in neuronal perikarya with little or no oligodendrocyte involvement 1 month post-injection. With longer post-injection survival intervals of up to 6 months, CBD-Tau- and AD-Tau-induced tau pathology spread to different brain regions distant from the injection sites while maintaining the cell type-specific pattern noted above. Finally, CA3 neuron loss was detected 3 months post-injection of AD-Tau but not CBD-Tau. Thus, AD-Tau and CBD-Tau represent specific pathological tau strains that spread differentially and may underlie distinct clinical and pathological features of these two tauopathies. Hence, these strains could become targets to develop disease-modifying therapies for CBD and AD.

trojanow@mail.med.upenn.edu.

Conflict of interest The authors declare that they have no conflict of interest.

Ethical standard All applicable international, national, and/ or institutional guidelines for the care and use of animals were followed. All procedures performed in studies involving animals were in accordance with the ethical standards of the institution or practice at which the studies were conducted.

Keywords

Alzheimer's disease; Corticobasal degeneration; Seeded transmission of pathological tau; Frontotemporal degeneration

Introduction

Alzheimer's disease (AD), corticobasal degeneration (CBD), progressive supranuclear palsy (PSP), argyrophilic grain disease (AGD) and Pick's disease (PiD) are neurodegenerative tauopathies characterized by different clinical features as well as distinct topographic and cell type-specific tau pathologies [2, 29]. Tau is predominantly an axonal microtubule-associated protein expressed as 6 alternatively spliced isoforms encoded by the tau gene (*MAPT*) with 3 (3R tau) versus 4 (4R tau) microtubule (MT)-binding repeats and 0 (0N), 1 (1N) or 2 (2N) amino terminal inserts resulting in 4R0N, 4R1N, 4R2N, 3R0N, 3R1N and 3R2N tau proteins at a 1:1 ratio of 3R to 4R tau in the adult CNS [2, 29]. Tau promotes MT assembly as well as stability, and while young tau knockout mice appear normal, aged knockout mice show synapse loss and cognitive impairments [36]. In the disease state, tau is hyperphosphorylated [28], nitrated [17], acetylated [8, 20, 21, 38] and glycosylated [26, 37] which may contribute to disease. While all 6 tau isoforms contribute to tau pathology in AD, 4R tau isoforms predominate in CBD, AGD and PSP, and 3R tau isoforms predominate in PiD [11, 39, 54–56]. The identification of >40 *MAPT* mutations pathogenic for familial tauopathies indicates that pathological tau alone is sufficient to cause neurodegeneration [2, 18, 44, 47, 48, 53].

It is known that pathological tau is taken up by cells and seeds aggregation of endogenous tau to form AD-like paired helical filaments (PHFs) or neurofibrillary tangles (NFTs) [9, 12, 14]. Further, injections of brain extracts from mutant human tau Tg mice harboring NFTs into the brains of Tg mice overexpressing wild-type human tau (ALZ17 line) induced tau inclusions [7], while injections of synthetic preformed tau fibrils (PFFs) into PS19 mice over-expressing mutant human tau induced similar tau pathology [19] indicating that tau PFFs alone are sufficient to transmit tau pathology. These and other studies suggest that pathological tau propagates to neighboring normal cells or those that are synaptically interconnected [1, 10, 35].

Since distinct tau strains may underlie diverse manifestations of neurodegenerative tauopathies [6, 45], we characterized the differential topography, cell spreading and consequences of tau pathology induced in the PS19 mice after injections of enriched pathological tau preparations from CBD (CBD-Tau) or AD (AD-Tau) brains and showed that this resulted in striking CBD-like or AD-like tau pathology that we attribute to different specific tau strains in CBD-Tau and AD-Tau.

Materials and methods

Tg Mice

Line PS19 Tg mice overexpressing the T34 isoform of tau (4R1N) encoding the P301S *MAPT* mutation driven by the murine prion protein promoter [52] were used in the studies

described here. The PS19 line at Penn was maintained on a B6C3 background, but as recently reported [19] and reviewed elsewhere (http://www.alzforum.org/research-models/tau-p301s-line-ps19), the onset of neurodegenerative tauopathy in the PS19 Tg mice at Penn has shifted from 6 to about 12 months of age thereby allowing a longer time window for the transmission studies described here.

Generation of enriched pathological tau from CBD and AD brains

Brain extracts from two longitudinally followed and autopsy confirmed CBD subjects as well as one AD patient and one elderly individual with Down syndrome (DS) whose brain contained abundant NFTs indistinguishable from AD, so we refer to this here as DSAD [28], were prepared. Brain extracts from a non-demented patient who showed no signs of neurodegenerative disease and no AD neuropathologic change at postmortem histological examination were used to generate normal or control tau (CTRL-Tau) preparations. All procedures were done sterile and at 4 °C.

For the preparation of CBD-Tau and CTRL-Tau, 400 mg of cortical gray matter from histologically confirmed cases of CBD and CTRL subjects were homogenized in 10 % PBS (W/V), briefly sonicated with an ultrasonic liquid processor (QSonica Microson™ XL-2000; 10 pulses; setting 2; 0.5 s/pulse) and centrifuged at 3,000*g* for 5 min (Beckman Coulter Optima™ MAX Ultracentrifuge). The resulting supernatant was centrifuged again at 100,000*g* for 30 min, following which the pellet was re-suspended in PBS in 1/3 of the initial volume, briefly sonicated and centrifuged again at 100,000*g* for 60 min. The resulting pellet was resuspended in PBS at 50 % of the initial volume. The pellet was sonicated, aliquoted, snap-frozen and stored at −80 °C until use.

The pathological AD-Tau- and DSAD-Tau-enriched preparations were processed from histologically confirmed AD and DSAD cases following a modified sucrose gradient protocol for the purification of AD PHFs [31]. Briefly, 50 g of frozen cortical gray matter was dissected, homogenized in 4 volumes of high-salt (H–S) RAB buffer (RAB buffer: 100 mM MES, 1 mM EDTA, 0.5 mM $MgSO_4$, 2 mM DTT, pH 6.8 + 0.75 M NaCl), incubated for 30 min on ice to depolymerize MTs and centrifuged at 126,000*g* for 45 min to remove soluble tau. The resulting pellet was used to generate AD-Tau by differential centrifugation, extraction with Sarkosyl and boiling to remove contaminants, followed by fractionation using a step-wise sucrose gradient to enrich for pathological AD-Tau [31]. AD-Tau was most enriched between the 1.75 and 2.00 M sucrose interface after over-night centrifugation and this material was collected and washed after which its purity was verified (see below).

Western blot analysis

The purity of enriched CBD-Tau and AD-Tau as well as the lack of pathological tau in the normal CTRL-Tau preparations was confirmed using Coomassie blue stained 7.5 % SDS-PAGE gel. The total protein loaded was 18 μg for CTRL, 22 μg for CBD-1, 26 μg for CBD-2, 32 μg for DSAD and 26 μg for AD. The same samples were analyzed by immunoblotting using anti-tau antibodies that recognize a phosphorylation-independent anti-tau polyclonal anti-body raised to recombinant tau (17025, 1:2,000; produced in the Penn Center for Neurodegenerative Disease Research (CNDR); [52]) and PHF tau phosphorylated

at Ser 396/404 (monoclonal antibody (mAb) PHF-1, 1:1,000; a gift of Peter Davies; [41]) as shown in Fig. 1.

Tau enzyme-linked immunosorbent assay (ELISA)

To determine total tau concentration in the fractions enriched in CBD-Tau, AD-Tau, DSAD-Tau and CTRL-Tau, we performed sandwich ELISA with anti-tau mAb Tau 5 as the capturing antibody in combination with mAbs HT7/ BT2 (Thermo-Scientific) for the reporter antibodies, as previously described [14].

Stereotaxic surgery

All experiments were performed in accordance with protocols approved by the Institutional Animal Care and Use Committee of the University of Pennsylvania. Briefly, 2 to 5 month old PS19 mice of either gender were deeply anesthetized with a ketamine/xylazine/acepromazine mixture, immobilized in a stereotaxic frame (David Kopf Instruments), following which different brain extracts were injected stereotaxically into the hippocampus and overlying neocortex using predetermined coordinates for hippocampus (Bregma −2.5 mm, lateral +2 mm, and depth −2 mm from brain surface) and overlying cortex (Bregma −2.5 mm, lateral +2 mm and depth −0.8 mm from brain surface) with a 10 μl Hamilton syringe under aseptic conditions as described [19]. All injected mice were observed during and after surgery. The total volume injected per site was 2.5 μl for all mice. The mice used for each experimental condition are summarized in Table 1.

Histology and immunohistochemistry (IHC)

At 1, 3 and 6 months post-injection, mice were sacrificed and their brains were fixed and processed as reported [19]. IHC was conducted on mouse brain sections incubated with primary antibodies followed by a polymer horseradish peroxidase detection system (Biogenex) and counterstained with hematoxylin. For semiquantitative IHC studies, every 20th slide from the serially sectioned mouse brains was immunostained with mAb AT8 (specific for tau phosphorylated at Ser202/Thr205; 1:10,000; Thermo-Scientific) and mAb MC1 (specific for a pathologic conformation of tau; 1:8,000; a gift from Peter Davies; [22]). Other anti-tau antibodies used in this study include: TG3 (specific for a conformation-dependent phosphorylated tau epitope; 1:250; a gift from Peter Davies; [23]), mAb T49, CNDR (specific for mouse tau; 1:2,000; [52]) and mAb T14, CNDR (specific for human tau, amino acids 141–178; 1:1,000; [25]). We also used 3R (RD3 1:2,500-5,000; Millipore, Billerica, MA, USA) and 4R (RD4 1:5,000-10,000; Millipore, Billerica, MA, USA) tau isoform-specific antibodies as described earlier [20]. Other antibodies used include mAb 81A, CNDR (specific for α-synuclein phosphorylated at Ser129; 1:50,000; [51]), mAb 409/410-TDP-43 (phosphorylation dependent at amino acids 409/410; 1:200; [40]), mAb NAB228, CNDR (antibody specific for $A\beta_{1-11}$: 1:60,000 with formic acid pre-treatment; [27]), Olig2 (specific for oligodendrocytes; 1:250, Millipore), a rat anti-glial fibrillary acidic protein (GFAP) mAb, CNDR (specific for astrocytes; 1:1,000; clone 2.2B10; [30]) and pAb, Iba-1 (specific to microglia; 1:1,000; Wako Chemicals).

Double-label immunofluorescence studies were used to identify glial cells with tau pathology as described [19]. To assess the amyloid properties of the tau inclusions induced

by CBD-Tau, AD-Tau and DSAD-Tau, sections were also stained with the Thioflavin S (ThS) amyloid-binding dye as described [19].

Quantification and statistics

We quantified the extent of glial tau pathology spread following injections with CBD-Tau in PS19 mice in a semi-quantitative manner (0: none; 1+: scant; 2+: moderate; 3+: abundant) where 1+ is rare (at least two tau inclusion bearing oligodendrocytes in a section) to a low burden of glial tau pathology and 3+ represents the presence of at least 25 tau-positive oligodendrocytes in a section. The tau pathology spread in the PS19 mice injected with AD-Tau and DSAD-Tau was more abundant than the CBD-Tau-injected mice, but they were very similar to each other and they were evaluated semiquantitatively (0: none; 1+: scant; 2+: moderate; 3+: abundant) as a single group. Scant (1+) tau pathology represents the presence of at least two tangle-bearing neurons in a particular region of a section and low neuritic tau pathology. Abundant (3+) represents >50 tau-positive neurons in a region of a section or abundant neuritic tau pathology. The same criteria were used for the assessment of the serial dilution assay of DSAD-Tau-injected mice. The topographical distribution of the tau pathology following CBD-Tau and AD-Tau or DSAD-Tau injections was used to generate heatmaps as described [19].

To evaluate neuron loss, we assessed a defined portion of the CA3 and CA1 region of matched brain sections stained with hematoxylin and eosin (H&E) from PS19 mice injected with AD-Tau or DSAD-Tau (n = 7 per time point), CBD-Tau (n = 6 per time point) and CTRL-Tau (n = 2 per time point) at 1, 3 and 6 months post-injection using 20× images. Neurons were individually counted using ImageJ software (National Institutes of Health). To determine statistical differences between groups, one-way ANOVA and Tukey's multiple-comparison test were used.

Results

Injections of CBD-Tau and AD-Tau induce tau pathology in PS19 Tg mice

To investigate whether pathological tau from different tauopathy brains induce distinct tau pathologies, we generated CTRL-Tau, CBD-Tau, AD-Tau or DSAD-Tau enriched preparations from the brains of a CTRL subject and 4 patients afflicted with these tauopathies, respectively, and then we injected them into the right hippocampus and overlying cortex of PS19 Tg mice (2–5 months old) (Table 1) after which we examined the resulting tau pathology at 1, 3 and 6 months post-injection intervals (Figs. 2, 3, 4). Mice developed pathology as early as 1 month after injection. PS19 mice injected with CBD-Tau induced predominantly glial tau pathology in white matter tracts and hippocampus close to the injection site at the earliest post-injection time point as detected by mAb AT8 (Fig. 2a, c, e). At 1 month post-injection, AT8-positive tau inclusions were seen in oligodendrocytes of the adjacent hippocampal fimbria (4/6; 66 % of mice) as well as in the alveus/ subcortical white matter/external capsule contiguous with the injection site (3/6; 50 % of mice) (Fig. 2, 3). Neurons in hippocampal regions CA1, CA3, dentate gyrus and subiculum also showed some perikaryal tau inclusions (Fig. 2e), but they were scant compared to the oligodendrocytes with tau pathology in the fimbria (Fig. 2c). They also were infrequent

compared to the large numbers of tangle-bearing neurons seen in the AD-Tau and DSAD-Tau injected mice (Fig. 2b, d, f) described below. Oligodendroglial tau inclusions extended beyond the injection site to rostral and caudal regions of the brain quite distal from the injection site (Fig. 3b). Infrequent or sparse intraneuronal tau inclusions in the hippocampus were also seen rostral and caudal to the injection site. Additionally, a small number of AT8 immunoreactive neurons were seen in the supramammillary bodies (data not shown). At 1 month post-injection, the tau inclusion pathology was limited to the side of the injection site, however, no tau pathology was seen in the overlying cortex even near these cortical injection sites. Finally, similar results were obtained when CBD-Tau from a second case with a confirmed CBD neuropathological diagnosis was injected in another cohort of mice (Table 1).

We next injected AD-Tau and DSAD-Tau into the brains of young PS19 mice which also showed prominent tau pathology at 1 month post-injection. Since the distribution of tau pathology in mice injected with AD-Tau and DSAD-Tau is very similar and the burden of AD pathology in both brains was similar, the data generated with these extracts were considered together as the AD/DSAD group. However, in contrast to the CBD-Tau-injected mice, the AD/DSAD-Tau-injected mice showed tau pathology mainly in perikarya and processes of hippocampal neurons (Fig. 2b, d, f). Mapping the spread of pathological tau from the hippocampal injection site over time post-injection in the AD/ DSAD-Tau injected mice demonstrated that the tau pathology extended to rostral and caudal regions of the brain (Fig. 4). In rostral areas, lateral septal nuclei were involved bilaterally with a moderate burden of tau inclusions in the processes of neurons. In caudal brain regions such as the subiculum, entorhinal cortex (EC) (Fig. 4), locus coeruleus (LC) and raphe nuclei, there also were AT8-positive neuronal aggregates (data not shown). Additionally, intracytoplasmic hyperphosphorylated tau inclusions were seen in the supramammillary nuclei (5/8; 63 % of mice) and in neocortex (4/8; 50 % of mice). Moreover, neuronal tau inclusion pathology was seen in the contralateral hemisphere where it was mainly limited to hippocampal neurons, with a predominance of involvement of CA3 region, and a few AT8-positive neurons in the EC. As in the ipsilateral side, intraneuronal tau pathology extended to rostral and caudal regions of the brain. Notably, no oligodendrocytic tau pathology was seen 1 month post-injection in the fimbria or the subcortical white matter/external capsule following AD/ DSAD-Tau injections. Finally, the tau pathology detected in these studies was exclusively 4R immunoreactive as would be expected in the PS19 that do not express any 3R tau.

As noted above, our non-injected PS19 mice begin to show transgene-driven tau pathology at ~12 months of age [19]. To control for this onset of transgene-driven tau pathology, we injected four young (2- to 3-month-old) PS19 mice with CTRL-Tau intracerebrally and these mice did not show any tau pathology at 1 or 6 months post-injection (data not shown).

Finally, none of the CBD-Tau- or AD/DSAD-Tau-injected PS19 mice showed any evidence of α-synuclein, TDP-43 or β-amyloid pathology despite the fact that these pathologies co-occur in AD/DSAD brains [32–34].

Tau pathology induced by CBD-Tau and AD/DSAD-Tau injections into young PS19 mice spread and increase with time

We assessed the progression of transmission of tau pathology with increasing survival times in PS19 mice following intracerebral injections of CBD-Tau and AD/ DSAD-Tau. The remarkable oligodendroglial tau pathology seen at 1 month post-injection in the CBD-Tau-injected Tg mice increased in the fimbria near and distal to the injection site at 3 months, and more so at 6 months post-injection (Fig. 3). Despite the variability in the burden of this oligodendroglial tau pathology, the PS19 mice that survived for 3 and 6 months post-injection displayed a clear increase in oligodendroglial tau pathology with time. Additionally, oligodendrocytic tau pathology spread to the contralateral fimbria although it was not as abundant as on the ipsilateral side (Fig. 3b). At 6 months post-injection, astrocytic-like plaques that closely resemble those seen in authentic human CBD brains were prominent in the stratum radiatum of the hippocampus in both hemispheres (Fig. 3a). Similarly, PS19 tau Tg mice injected with AD/DSAD-Tau showed an increase in the neuronal tau pathology burden as well as prominent spread to regions quite distal from the injection site with increasing post-injection survival times (Fig. 4). However, this pattern of neuronal spread, which is consistent with intra-axonal transmission, differed dramatically from the pattern of glial tau pathology spread seen following the CBD-Tau injections, suggestive of a different mode of transmission that does not depend on the axonal afferents and efferents of the injection sites like the AD/ DSAD-Tau injections.

At 3 months post-injection, there was an increase of the pathology in the regions that were already involved at 1 month post-injection. In the ipsilateral side, the dentate gyrus (DG) showed an increase in neuronal tau pathology at 3 months that seemed to plateau at 6 months. In the CA1 region, there was variability in the burden of intra-neuronal tau inclusions at 1 month post-injection, but there was a decrease of pathology from 3 to 6 months post-injection. CA3 tau pathology also decreased from 1 to 6 months post-injection. In the contralateral hemisphere, hippocampal tau inclusions were less numerous, but they showed an increase in quantity with time in DG and CA1, while a reduction of tau pathology was observed in the CA3 region. Additionally, in keeping with the interpretation that the spread of AD/DSAD-Tau-induced tau pathology occurs through intra-axonal transport, tau pathology was seen in other regions that were not involved at earlier stages such as the thalamus, mammillary nuclei and other hypothalamic nuclei (Fig. 4b). At 3 months post-injection, neocortical neurons were involved in all of the AD/DSAD-Tau-injected mice. Additionally, some tau pathology appeared in white matter tracts with involvement of the fimbria and the dorsal hippocampal commissure at 3 months, and this pathology increased at 6 months post-injection where it appeared to be in astrocytes and oligodendroglia, but it never approached the abundance of the glial tau pathology induced by the CBD-Tau injections (data not shown). However, at 6 months post-injection there was a decrease in NFT pathology in the majority of affected areas in the AD/DSAD-Tau-injected mice.

Tau pathology induced by AD/DSAD-Tau, but not CBD-Tau injections into young PS19 mice results in neuron loss with time

To determine if the decreasing NFT pathology seen in the hippocampal region of AD/ DSAD-Tau injected PS19 mice may be due to neuron loss, we quantified the number of

CA3 neurons, in the area delimited by the rectangle, on the side contralateral to the injection site using digital micrography. As shown in Fig. 5, fewer neurons were seen in CA3 at the 1–3 months post-injection time period compared to controls, but this loss of neurons did not progress further as it stabilized at the 6 months post-injection survival time [138 ± 6 cell, 74 ± 7 and 69 ± 3 neurons at 1, 3 and 6 months, respectively; $p < 0.001$; (Fig. 5b)]. In marked contrast, no neuron loss was seen in mice injected with CBD-Tau (128 ± 5, 126 ± 5, 129 ± 9 neurons at 1, 3 and 6 months, respectively) or CTRL-Tau injected mice (129, 130 ± 9 neurons at 1 and 6 months, respectively). Additionally, we analyzed the CA1 region of the hippocampus on the contralateral side of the injection site but no neuron loss was observed at any of the post-injection survival time points for mice injected with AD/DSAD-Tau (330 ± 13, 321 ± 36, 318 ± 25 neurons at 1, 3 and 6 months, respectively), CBD-Tau (301 ± 17, 303 ± 32, 325 ± 30 neurons at 1, 3 and 6 months, respectively) or CTRL-Tau (286 ± 13, 330 ± 5 neurons at 1 and 6 months, respectively) (data not shown).

We further studied the association of the neuron loss with reactive changes to neurodegeneration and we observed an increase in astrogliosis in the CA3 region of the hippocampus associated with the loss of neurons, however, microgliosis was less intense.

The burden and distribution of DSAD-Tau-induced tau pathology is dose dependent

The abundance of neuronal tau inclusions induced in the PS19 mice with synthetic tau PFF injections was not only time dependent as described above, but following injections of increasing amounts of recombinant P301S mutant human T40 tau (T40/PS) PFFs, the induced pathology increased in a dose-dependent manner as well [19]. Thus, we investigated this dose dependency here by injecting serially diluted DSAD-Tau into the hippocampus and overlying neocortex of PS19 mice (Table 1) and analyzing the tau pathology at 1 month after injection. As shown schematically in Fig. 6, at the lowest concentration of injected DSAD-Tau, only the ipsilateral hippocampus showed induced tau pathology. AT8-positive inclusions in the perikarya of neurons of dentate gyrus, CA3 and CA1 were seen at the injection site and also in rostral and caudal regions of the hippocampus of the ipsilateral side. The burden of tau pathology in the hippocampus increased with increasing concentrations of injected pathological tau with other regions of the brain becoming involved with increasing DSAD-Tau concentrations (Fig. 6). Inclusions in the contralateral hemisphere also developed in a dose-dependent manner. Hence, at the lowest concentrations of DSAD-Tau, there was no tau pathology on the contralateral side of the PS19-injected mice, while higher concentrations of injected pathological tau induced more tau pathology in the contralateral CA3 region. In sharp contrast to the CBD-Tau injected at 1 month post-injection, there was no tau pathology in the ipsilateral or contralateral white matter tracts at any concentration of injected DSAD-Tau at 1 month post-injection.

CBD-Tau- and AD/DSAD-Tau-induced tau pathology acquires the key characteristics of their human counterparts

We further characterized the nature of the CBD-Tau- and AD/DSAD-Tau-induced tau pathology in PS19 mice by performing IHC using anti-tau mAbs to pathological tau that detect human CBD and AD-Tau pathology. IHC with MC1 and TG3 showed that tau inclusions induced by CBD-Tau was modestly positive for both mAbs at 1 month post-

injection, but detected more intense and abundant tau pathology at 3 months which increased further by 6 months post-injection (Fig. 7). By contrast, AD/DSAD-Tau-induced tau pathology was intensely immunoreactive for both MC1 and TG3 already at 1 month post-injection. Notably, human (T14) and mouse (T49) specific anti-tau mAbs stained all of the tau pathologies described above although T49 stained oligoden-droglial tau pathology very weakly (data not shown).

Since AD NFTs are detected by amyloid-binding dyes such as ThS, while tau inclusions in CBD cases are ThS negative [46], we asked if these properties of tau aggregates persisted in our PS19 mice following injections with CBD-Tau and AD/DSAD-Tau. Remarkably, the tau pathology in mice, injected with human-derived CBD-Tau that were AT8 positive, did not show ThS positivity, even at 6 months after injection, however, tau inclusions appearing only 1 month post-injection with AD/DSAD-Tau were detected by ThS (Fig. 7). Thus, human CBD-Tau and AD/DSAD-Tau templated and propagated tau pathology in the injected PS19 mice that showed compelling immunological and histochemical verisimilitude to their human counterparts.

Further evidence of this verisimilitude came from double immunofluorescence studies showing that the CBD-Tau-induced pathology was double labeled with AT8 and Olig2 mAbs confirming the oligodendroglial nature of this oligodendroglial tau pathology while the astrocytic plaques induced by the CBD-Tau showed partial or incomplete co-localization of AT8 and GFAP similar to what is seen in the astrocytic plaques of human CBD (Fig. 8) as described [16].

Discussion

Here, we substantially extend the prior studies of Clavaguera et al. [6] by showing that intracellular tau pathology rapidly develops within 4 weeks rather than within several months in a Tg mouse model (line PS19) overexpressing P301S mutant human 4R1N tau after intracerebral injections of brain extracts enriched in CBD-Tau, AD-Tau or DSAD-Tau. We confirm the earlier findings [6] that this tau pathology is largely cell type specific and recapitulates the specific features of CBD or AD Tau pathology following injections of CBD-Tau or AD/DSAD-Tau, respectively. Thus, while the tau inclusions induced by CBD-Tau predominantly developed in oligodendrocytes with some astrocytic plaques, similar to authentic CBD-Tau pathology, the tau inclusions induced by AD/DSAD-Tau formed mainly in neurons similar to the NFTs in AD and DSAD brains. However, we significantly extended the initial report of Clavaguera et al. [6] by biochemically characterizing the pathological tau, we injected in more detail and demonstrating that the induction and spread of this tau pathology is time as well as dose dependent, and in the case of AD/DSAD-Tau, this tau pathology is associated with time-dependent neuron loss in the CA3 region while no similar neuron loss was seen in the CBD-Tau injected mice. Moreover, we also used antibodies to specific pathological tau conformations as well as ThS staining and double-label immunofluorescence with AT8 and Olig2 and GFAP antibodies to extend the comparison of the human CBD and AD/DSAD pathologies to the tau pathologies induced in the PS19 tau Tg mice injected with CBD-Tau or AD/DSAD-Tau, respectively. Thus, we report novel data indicating that while CBD-Tau and AD/DSAD-Tau induced dramatically

different tau pathology in the PS19 mice, CBD-Tau- and AD/DSAD-Tau-induced tau pathology shows remarkable verisimilitude to human CBD and AD-Tau pathology, respectively.

While the AD-like tau pathology spreads in a manner consistent with dissemination through the connectome of the injected brain regions, most likely via intra-axonal transport, the manner in which the CBD glial tau pathology spreads is enigmatic and will require further studies to elucidate. Indeed, while there are staging schemes for AD-Tau pathology that support the notion of tau pathology spread through interconnected brain regions [3–5], no similar staging exists for CBD-Tau pathology so it is not clear how tau pathology might progress and spread in CBD brains. The fact that injections of brain extracts from control non-diseased human brains lacking any insoluble pathological tau did not induce tau pathology in age-matched PS19 mice support data from a growing number of studies indicating that pathological tau and not normal tau induce the seeded transmission and spread of pathological tau in vivo and in vitro (for reviews, see [15, 24]).

Transmission of tau pathology in vitro was demonstrated initially using AD brain extracts that induced formation of PHFs in cultured fetal neurons [9] and later used synthetic tau PFFs to induce the templated conversion of intracellular soluble tau into fibrillar aggregates in cultured cells [12, 14]. In vivo studies showed that inoculation of brain homogenates from mutant tau Tg mice (that form NFTs) into the brains of WT tau expressing ALZ17 mice (that do not form tau inclusions) induced the formation of tau inclusions in the ALZ17 Tg mice [7]. Iba et al. [19] demonstrated that synthetic tau fibrils injected into a PS19 tauopathy model is sufficient to induce and propagate AD-like tau pathology. Altogether, it was established that fibrillar species of tau are capable of recruiting and converting endogenous soluble tau into pathological aggregates in neurons and neuronal processes in vivo. In our present study, we showed that enriched pathological tau extracts obtained from CBD or AD and DSAD brains induce tau pathology in PS19 mice similar to CBD and AD Tau pathology in human brains, respectively. These results support the notion that different tauopathy-specific pathological tau strains may account for the diverse clinical and pathological phenotypes of tauopathy variants. Moreover, our mouse model differs from the initial report of Clavaguera et al. [6] in that the tau pathology in our model developed earlier and showed a striking verisimilitude to key features of CBD or AD Tau pathology following injections of CBD-Tau or AD/ DSAD-Tau, respectively.

Some tauopathies characteristically show tau inclusions in glial cells and neurons [2, 29]. The basis of this cell-type preference for the formation of tau inclusions is unknown, but a recent study demonstrated in vitro and in vivo that pathological tau can acquire different conformations which propagate tau pathology suggesting that these different conformers or strains could result in the different tauopathies [45]. These characteristics have been also shown for α-synuclein [13] and Aβ [43, 49, 50]. Moreover, since tau inclusions in CBD and AD are formed by different tau isoforms (i.e. CBD is predominantly 4R; AD is predominantly 3R and 4R), this also might determine the structure of different tau strains. However, little is known about how different pathological tau isoforms contribute to the heterogeneous phenotypes seen in different tauopathies. That said, we observed that the injection of enriched tau extracts from AD and DSAD brains resulted in similar AD-like

neuronal tau pathologies while both the CBD cases produced distinctly different pathology from the AD/DSAD cases that was remarkably CBD like. Thus, these findings suggest that the characteristics and distributions of these different tau inclusions are directly related with the nature of the tauopathy.

Notably, the tau pathology seen in the hippocampus of PS19 tau Tg mice after the injection of AD/DSAD-Tau was variable and appeared to decrease in the CA3 region ipsilateral and contralateral to the injection and we showed that this could be explained by the neuron loss seen in this region that was already significant at 3 months post-injection (Fig. 5). It is noteworthy that the CA3 region in the injected PS19 mice develops neuronal tau inclusions at 1 month post-injection, and is one of the first regions to show AT8-positive inclusions in the contralateral hippocampus preceding neuronal death. Thus, it is possible that distinct tau species have a differential effect in the neurons of these mice causing neuronal death and this may occur in a neuron type-specific manner or could be dose and time dependent, as might be inferred from a recently published study in which high doses of synthetic tau fibrils caused hippocampal neuron death [42]. For comparison, we also analyzed neuron loss in the CA1 region of the hippocampus contralateral to the injection site, where tau inclusions were less abundant than in CA3 and no neuron loss was observed. Interestingly, neuron loss in the CA3 region was accompanied by moderate astrogliosis and less conspicuous microgliosis, which is evidence of reactive changes to this neurodegeneration.

Other data support the verisimilitude of the CBD-Tau- and AD/DSAD-Tau-induced tau pathology in the injected PS19 mice to their human counterparts in CBD and AD, respectively. For example, the inclusions resulting in oligodendrocyte pathology in the fimbria after injection of human-derived CBD-Tau were positive for the conformational antibody MC1 while a few inclusions showed TG3 immunoreactivity. Interestingly, ThS was negative even at 6 months after injection which is a characteristic of tau inclusions in human CBD [46]. In contrast, in the AD/ DSAD-Tau-injected mice there was an intense immunore-activity for MC1 and TG3 and positivity for ThS staining already at 1 month after injection, indicating more mature NFT structures analogous to what is seen in AD patients at histological examination.

In conclusion, we present mouse models of CBD-like and AD-like tauopathies that rapidly develop glial and intraneuronal tau inclusions after the injection of pathological tau isolated from CBD or AD/DSAD brains, respectively, and also rapidly progress in a stereotypical pattern. For AD/DSAD-Tau, this progression is both time and dose dependent as well as dependent on the connectome of the injection sites. Notably, this tau pathology leads to the death of tangle-bearing CA3 neurons over time. In sharp contrast, the spread of CBD-Tau-induced tau pathology in glial cells was more limited as well as unrelated to the connectome of the injection site and it did not appear to cause the loss of neurons or glial cells. Thus, we anticipate that these models will provide informative systems for studies on the transmission of tau pathology, tau-mediated neuronal and glial degeneration and the development of disease-modifying therapies for CBD and AD.

Acknowledgments

Susana Boluda was supported by Bolsa de Ampliación de Estudios (BA11/00021) from the Spanish government, Instituto de Salud Carlos III, Ministerio de Ciencia e Innovación, Madrid, Spain. This work was supported by the CurePSP Foundation, NIH grant AG17586, the Marian S. Ware Alzheimer Program, the Karen Cohen Segal, the Eleanor Margaret Kurtz Endowed Fund, the Mary Rasmus Endowed Fund for Alzheimer's Research, Mrs. Gloria J. Miller and Arthur Peck, M.D. We thank Theresa Schuck, John Robinson and Jennifer McBride for their technical assistance in immunohistochemistry, Linda Kwong for her technical assistance in biochemistry procedures and reading of this manuscript, Sue Leight for her technical assistance in mouse manipulation, Magdalena Nitla for her technical assistance in mouse injections and Young Baek and Rui Tong for data management.

References

1. Ahmed Z, Cooper J, Murray TK, Garn K, McNaughton E, Clarke H, Parhizkar S, Ward MA, Cavallini A, Jackson S, Bose S, Clavaguera F, Tolnay M, Lavenir I, Goedert M, Hutton ML, O'Neill MJ. A novel in vivo model of tau propagation with rapid and progressive neurofibrillary tangle pathology: the pattern of spread is determined by connectivity, not proximity. Acta Neuropathol. 2014; 127(5):667–683. [PubMed: 24531916]
2. Ballatore C, Lee VM, Trojanowski JQ. Tau-mediated neurodegeneration in Alzheimer's disease and related disorders. Nat Rev Neurosci. 2007; 8(9):663–672. doi:10.1038/nrn2194. [PubMed: 17684513]
3. Braak H, Braak E. Neuropathological stageing of Alzheimer-related changes. Acta Neuropathol. 1991; 82(4):239–259. [PubMed: 1759558]
4. Braak H, Del Tredici K. Alzheimer's pathogenesis: is there neuron-to-neuron propagation? Acta Neuropathol. 2011; 121(5):589–595. [PubMed: 21516512]
5. Braak H, Thal DR, Ghebremedhin E, Del Tredici K. Stages of the pathologic process in Alzheimer disease: age categories from 1 to 100 years. J Neuropathol Exp Neurol. 2011; 70(11):960–969. [PubMed: 22002422]
6. Clavaguera F, Akatsu H, Fraser G, Crowther RA, Frank S, Hench J, Probst A, Winkler DT, Reichwald J, Staufenbiel M, Ghetti B, Goedert M, Tolnay M. Brain homogenates from human tauopathies induce tau inclusions in mouse brain. Proc Natl Acad Sci. 2013; 110(23):9535–9540. [PubMed: 23690619]
7. Clavaguera F, Bolmont T, Crowther RA, Abramowski D, Frank S, Probst A, Fraser G, Stalder AK, Beibel M, Staufenbiel M, Jucker M, Goedert M, Tolnay M. Transmission and spreading of tauopathy in transgenic mouse brain. Nat Cell Biol. 2009; 11(7):909–913. [PubMed: 19503072]
8. Cohen TJ, Guo JL, Hurtado DE, Kwong LK, Mills IP, Trojanowski JQ, Lee VM. The acetylation of tau inhibits its function and promotes pathological tau aggregation. Nat Commun. 2011; 2:252. [PubMed: 21427723]
9. De Boni U, Crapper DR. Paired helical filaments of the Alzheimer type in cultured neurones. Nature. 1978; 271(5645):566–568. [PubMed: 622193]
10. de Calignon A, Polydoro M, Suarez-Calvet M, William C, Adamowicz DH, Kopeikina KJ, Pitstick R, Sahara N, Ashe KH, Carlson GA, Spires-Jones TL, Hyman BT. Propagation of tau pathology in a model of early Alzheimer's disease. Neuron. 2012; 73(4):685–697. [PubMed: 22365544]
11. Forman MS, Zhukareva V, Bergeron C, Chin SSM, Grossman M, Clark C, Lee VMY, Trojanowski JQ. Signature tau neuropathology ingray and white matter of corticobasal degeneration. Am J Pathol. 2002; 160(6):2045–2053. doi:10.1016/ s0002-9440(10)61154-6. [PubMed: 12057909]
12. Frost B, Jacks RL, Diamond MI. Propagation of tau misfolding from the outside to the inside of a cell. J Biol Chem. 2009; 284(19):12845–12852. [PubMed: 19282288]
13. Guo JL, Covell DJ, Daniels JP, Iba M, Stieber A, Zhang B, Riddle DM, Kwong LK, Xu Y, Trojanowski JQ, Lee VM. Distinct alpha-synuclein strains differentially promote tau inclusions in neurons. Cell. 2013; 154(1):103–117. [PubMed: 23827677]
14. Guo JL, Lee VM. Seeding of normal tau by pathological tau conformers drives pathogenesis of Alzheimer-like tangles. J Biol Chem. 2011; 286(17):15317–15331. [PubMed: 21372138]

15. Guo JL, Lee VM. Cell-to-cell transmission of pathogenic proteins in neurodegenerative diseases. Nat Med. 2014; 20(2):130–138. doi:10.1038/nm.3457. [PubMed: 24504409]
16. Higuchi M, Zhang B, Forman MS, Yoshiyama Y, Trojanowski JQ, Lee VM. Axonal degeneration induced by targeted expression of mutant human tau in oligodendrocytes of transgenic mice that model glial tauopathies. J Neurosci. 2005; 25(41):9434–9443. [PubMed: 16221853]
17. Horiguchi T, Uryu K, Giasson BI, Ischiropoulos H, LightFoot R, Bellmann C, Richter-Landsberg C, Lee VM, Trojanowski JQ. Nitration of tau protein is linked to neurodegeneration in tauopathies. Am J Pathol. 2003; 163(3):1021–1031. [PubMed: 12937143]
18. Hutton M, Lendon CL, Rizzu P, Baker M, Froelich S, Houlden H, Pickering-Brown S, Chakraverty S, Isaacs A, Grover A, Hackett J, Adamson J, Lincoln S, Dickson D, Davies P, Petersen RC, Stevens M, de Graaff E, Wauters E, van Baren J, Hillebrand M, Joosse M, Kwon JM, Nowotny P, Che LK, Norton J, Morris JC, Reed LA, Trojanowski J, Basun H, Lannfelt L, Neystat M, Fahn S, Dark F, Tannenberg T, Dodd PR, Hayward N, Kwok JB, Schofield PR, Andreadis A, Snowden J, Craufurd D, Neary D, Owen F, Oostra BA, Hardy J, Goate A, van Swieten J, Mann D, Lynch T, Heutink P. Association of missense and 5′-splice-site mutations in tau with the inherited dementia FTDP-17. Nature. 1998; 393(6686):702–705. [PubMed: 9641683]
19. Iba M, Guo JL, McBride JD, Zhang B, Trojanowski JQ, Lee VM. Synthetic tau fibrils mediate transmission of neurofibrillary tangles in a transgenic mouse model of Alzheimer's-like tauopathy. J Neurosci. 2013; 33(3):1024–1037. [PubMed: 23325240]
20. Irwin DJ, Cohen TJ, Grossman M, Arnold SE, McCarty-Wood E, Van Deerlin VM, Lee VM, Trojanowski JQ. Acetylated tau neuropathology in sporadic and hereditary tauopathies. Am J Pathol. 2013; 183(2):344–351. [PubMed: 23885714]
21. Irwin DJ, Cohen TJ, Grossman M, Arnold SE, Xie SX, Lee VM, Trojanowski JQ. Acetylated tau, a novel pathological signature in Alzheimer's disease and other tauopathies. Brain. 2012; 135:807–818. Pt 3. [PubMed: 22366796]
22. Jicha GA, Bowser R, Kazam IG, Davies P. Alz-50 and MC-1, a new monoclonal antibody raised to paired helical filaments, recognize conformational epitopes on recombinant tau. J Neurosci Res. 1997; 48(2):128–132. [PubMed: 9130141]
23. Jicha GA, Lane E, Vincent I, Otvos L Jr, Hoffmann R, Davies P. A conformation- and phosphorylation-dependent antibody recognizing the paired helical filaments of Alzheimer's disease. J Neurochem. 1997; 69(5):2087–2095. [PubMed: 9349554]
24. Jucker M, Walker LC. Self-propagation of pathogenic protein aggregates in neurodegenerative diseases. Nature. 2013; 501(7465):45–51. [PubMed: 24005412]
25. Kosik KS, Orecchio LD, Binder L, Trojanowski JQ, Lee VM, Lee G. Epitopes that span the tau molecule are shared with paired helical filaments. Neuron. 1988; 1(9):817–825. [PubMed: 2483104]
26. Ledesma MD, Perez M, Colaco C, Avila J. Tau glycation is involved in aggregation of the protein but not in the formation of filaments. Cell Mol Biol. 1998; 44(7):1111–1116. [PubMed: 9846893]
27. Lee EB, Leng LZ, Zhang B, Kwong L, Trojanowski JQ, Abel T, Lee VM. Targeting amyloid-beta peptide (Abeta) oligomers by passive immunization with a conformation-selective monoclonal antibody improves learning and memory in Abeta precursor protein (APP) transgenic mice. J Biol Chem. 2006; 281(7):4292–4299. [PubMed: 16361260]
28. Lee VM, Balin BJ, Otvos L Jr, Trojanowski JQ. A68: a major subunit of paired helical filaments and derivatized forms of normal tau. Science. 1991; 251(4994):675–678. [PubMed: 1899488]
29. Lee VM, Goedert M, Trojanowski JQ. Neurodegenerative tauopathies. Annu Rev Neurosci. 2001; 24:1121–1159. [PubMed: 11520930]
30. Lee VM, Page CD, Wu HL, Schlaepfer WW. Monoclonal antibodies to gel-excised glial filament protein and their reactivities with other intermediate filament proteins. J Neurochem. 1984; 42(1): 25–32. [PubMed: 6358415]
31. Lee VM, Wang J, Trojanowski JQ. Purification of paired helical filament tau and normal tau from human brain tissue. Methods Enzymol. 1999; 309:81–89. [PubMed: 10507018]
32. Lippa CF, Fujiwara H, Mann DM, Giasson B, Baba M, Schmidt ML, Nee LE, O'Connell B, Pollen DA, St George-Hyslop P, Ghetti B, Nochlin D, Bird TD, Cairns NJ, Lee VM, Iwatsubo T, Trojanowski JQ. Lewy bodies contain altered alpha-synuclein in brains of many familial

Alzheimer's disease patients with mutations in presenilin and amyloid precursor protein genes. Am J Pathol. 1998; 153(5):1365–1370. [PubMed: 9811326]

33. Lippa CF, Rosso AL, Stutzbach LD, Neumann M, Lee VM, Trojanowski JQ. Transactive response DNA-binding protein 43 burden in familial Alzheimer disease and Down syndrome. Arch Neurol. 2009; 66(12):1483–1488. [PubMed: 20008652]
34. Lippa CF, Schmidt ML, Lee VM, Trojanowski JQ. Antibodies to alpha-synuclein detect Lewy bodies in many Down's syndrome brains with Alzheimer's disease. Ann Neurol. 1999; 45(3):353–357. [PubMed: 10072050]
35. Liu L, Drouet V, Wu JW, Witter MP, Small SA, Clelland C, Duff K. Trans-synaptic spread of tau pathology in vivo. PLoS One. 2012; 7(2):1.
36. Ma QL, Zuo X, Yang F, Ubeda OJ, Gant DJ, Alaverdyan M, Kiosea NC, Nazari S, Chen PP, Nothias F, Chan P, Teng E, Frautschy SA, Cole GM. Loss of MAP function leads to hippocampal synapse loss and deficits in the Morris Water Maze with aging. J Neurosci. 2014; 34(21):7124–7136. [PubMed: 24849348]
37. Martin L, Latypova X, Terro F. Post-translational modifications of tau protein: implications for Alzheimer's disease. Neurochem Int. 2011; 58(4):458–471. [PubMed: 21215781]
38. Min SW, Cho SH, Zhou Y, Schroeder S, Haroutunian V, Seeley WW, Huang EJ, Shen Y, Masliah E, Mukherjee C, Meyers D, Cole PA, Ott M, Gan L. Acetylation of tau inhibits its degradation and contributes to tauopathy. Neuron. 2010; 67(6):953–966. [PubMed: 20869593]
39. Mott RT, Dickson DW, Trojanowski JQ, Zhukareva V, Lee VM, Forman M, Van Deerlin V, Ervin JF, Wang DS, Schmechel DE, Hulette CM. Neuropathologic, biochemical, and molecular characterization of the frontotemporal dementias. J Neuropathol Exp Neurol. 2005; 64(5):420–428. [PubMed: 15892300]
40. Neumann M, Kwong LK, Lee EB, Kremmer E, Flatley A, Xu Y, Forman MS, Troost D, Kretzschmar HA, Trojanowski JQ, Lee VM. Phosphorylation of S409/410 of TDP-43 is a consistent feature in all sporadic and familial forms of TDP-43 proteinopathies. Acta Neuropathol. 2009; 117(2):137–149. [PubMed: 19125255]
41. Otvos L Jr, Feiner L, Lang E, Szendrei GI, Goedert M, Lee VM. Monoclonal antibody PHF-1 recognizes tau protein phosphorylated at serine residues 396 and 404. J Neurosci Res. 1994; 39(6):669–673. [PubMed: 7534834]
42. Peeraer E, Bottelbergs A, Van Kolen K, Mahieu M, Duytschaever H, Verdonck L, Torremans A, Andries L, Brunden KR, Trojanowski JQ, Lee VM, Dewachter I, Kemp JA, Moechars D. Intracerebral injection of tau aggregates initiates widespread tauopathy and neuronal loss in transgenic mouse brain. Neurobiol Dis. 2014; 73C:83–95. [PubMed: 25220759]
43. Petkova AT, Leapman RD, Guo Z, Yau WM, Mattson MP, Tycko R. Self-propagating, molecular-level polymorphism in Alzheimer's beta-amyloid fibrils. Science. 2005; 307(5707):262–265. [PubMed: 15653506]
44. Poorkaj P, Bird TD, Wijsman E, Nemens E, Garruto RM, Anderson L, Andreadis A, Wiederholt WC, Raskind M, Schellenberg GD. Tau is a candidate gene for chromosome 17 frontotemporal dementia. Ann Neurol. 1998; 43(6):815–825. [PubMed: 9629852]
45. Sanders DW, Kaufman SK, DeVos SL, Sharma AM, Mirbaha H, Li A, Barker SJ, Foley AC, Thorpe JR, Serpell LC, Miller TM, Grinberg LT, Seeley WW, Diamond MI. Distinct tau prion strains propagate in cells and mice and define different tauopathies. Neuron. 2014; 82(6):1271–1288. [PubMed: 24857020]
46. Schmidt ML, Schuck T, Sheridan S, Kung MP, Kung H, Zhuang ZP, Bergeron C, Lamarche JS, Skovronsky D, Giasson BI, Lee VM, Trojanowski JQ. The fluorescent Congo red derivative, (trans, trans)-1-bromo-2,5-bis-(3-hydroxycarbonyl-4-hydroxy)styrylbenzene (BSB), labels diverse beta-pleated sheet structures in postmortem human neurodegenerative disease brains. Am J Pathol. 2001; 159(3):937–943. [PubMed: 11549586]
47. Spillantini MG, Goedert M. Tau pathology and neurode-generation. Lancet Neurol. 2013; 12(6):609–622. [PubMed: 23684085]
48. Spillantini MG, Van Swieten JC, Goedert M. Tau gene mutations in frontotemporal dementia and parkinsonism linked to chromosome 17 (FTDP-17). Neurogenetics. 2000; 2(4):193–205. [PubMed: 10983715]

49. Stohr J, Condello C, Watts JC, Bloch L, Oehler A, Nick M, DeArmond SJ, Giles K, DeGrado WF, Prusiner SB. Distinct synthetic Abeta prion strains producing different amyloid deposits in bigenic mice. Proc Natl Acad Sci. 2014; 111:10329–10334. [PubMed: 24982137]
50. Stohr J, Watts JC, Mensinger ZL, Oehler A, Grillo SK, DeArmond SJ, Prusiner SB, Giles K. Purified and synthetic Alzheimer's amyloid beta (Abeta) prions. Proc Natl Acad Sci. 2012; 109(27):11025–11030. doi:10.1073/pnas.1206555109. [PubMed: 22711819]
51. Waxman EA, Giasson BI. Specificity and regulation of casein kinase-mediated phosphorylation of alpha-synuclein. J Neuropathol Exp Neurol. 2008; 67(5):402–416. [PubMed: 18451726]
52. Yoshiyama Y, Higuchi M, Zhang B, Huang SM, Iwata N, Saido TC, Maeda J, Suhara T, Trojanowski JQ, Lee VM. Synapse loss and microglial activation precede tangles in a P301S tauopathy mouse model. Neuron. 2007; 53(3):337–351. [PubMed: 17270732]
53. Yoshiyama Y, Lee VM, Trojanowski JQ. Therapeutic strategies for tau mediated neurodegeneration. J Neurol Neurosurg Psychiatry. 2013; 84(7):784–795. [PubMed: 23085937]
54. Zhukareva V, Joyce S, Schuck T, Van Deerlin V, Hurtig H, Albin R, Gilman S, Chin S, Miller B, Trojanowski JQ, Lee VM. Unexpected abundance of pathological tau in progressive supra-nuclear palsy white matter. Ann Neurol. 2006; 60(3):335–345. [PubMed: 16823854]
55. Zhukareva V, Mann D, Pickering-Brown S, Uryu K, Shuck T, Shah K, Grossman M, Miller BL, Hulette CM, Feinstein SC, Trojanowski JQ, Lee VM. Sporadic Pick's disease: a tauopathy characterized by a spectrum of pathological tau isoforms in gray and white matter. Ann Neurol. 2002; 51(6):730–739. [PubMed: 12112079]
56. Zhukareva V, Shah K, Uryu K, Braak H, Del Tredici K, Sundarraj S, Clark C, Trojanowski JQ, Lee VM. Biochemical analysis of tau proteins in argyrophilic grain disease, Alzheimer's disease, and Pick's disease: a comparative study. Am J Pathol. 2002; 161(4):1135–1141. [PubMed: 12368187]

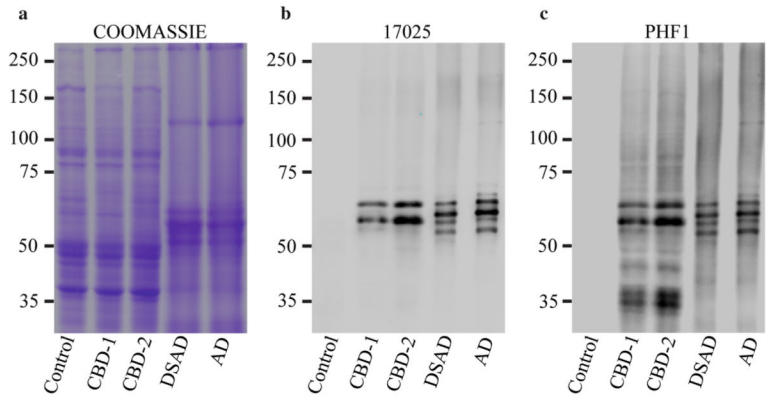

Fig. 1.

Biochemical analysis of the pathological tau protein-enriched extracts obtained from human brains with a neuropathological diagnosis of CBD, AD, DSAD and a non-disease normal control brain used for injection into PS19 Tg mice. SDS gel stained with *Coomassie blue* (**a**). Immunoblots stained with 17025 (**b**) and PHF1 (**c**)

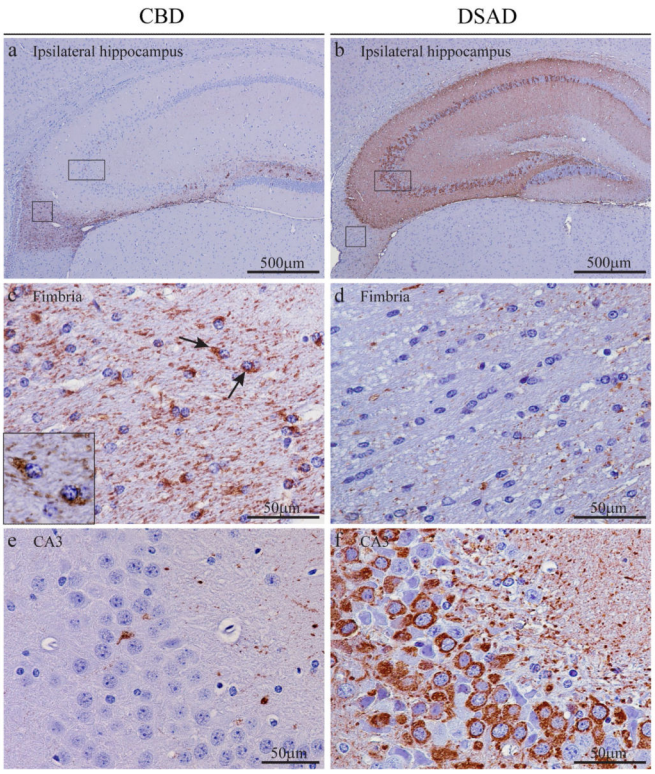

Fig. 2.

Development of cell type-specific tau inclusions after injection of CBD-Tau- or DSAD-Tau-enriched protein extracts into the brains of PS19 mice. **a**, **c**, **e** AT8-positive oligodendroglial inclusions developed in the fimbria of the hippocampus on the injected side at 1 month after the injection of CBD-Tau. **b**, **d**, **f** AT8-positive inclusions developed in the perikarya of neurons of the hippocampus of DSAD-Tau-injected mice. **c** A higher magnification of the *square boxed area* in (**a**) is shown in (**c**) demonstrating AT8-positive tau inclusions in many oligodendrocytes of the fimbria (**c**). The *inset* in (**c**) shows a detail of the oligodendrocytes indicated by the *black arrows*. **d** A higher magnification of the *square boxed area* in (**b**) is shown in (**d**) demonstrating the absence of tau inclusions in the oligodendrocytes of the fimbria (**d**) which contrasts with the CBD-Tau-injected mice. **e** Higher magnification of the *rectangular boxed area* in (**a**) demonstrating only rare intraneuronal inclusions in the CA3 region of the hippocampus (**e**). In **f**, where a higher magnification of the *rectangular boxed area* in (**b**) is depicted, there is abundance of perikaryal AT8 inclusions in CA3 of the hippocampus. *Scale bar*, *upper row* 500 μm; *middle* and *bottom rows* 50 μm

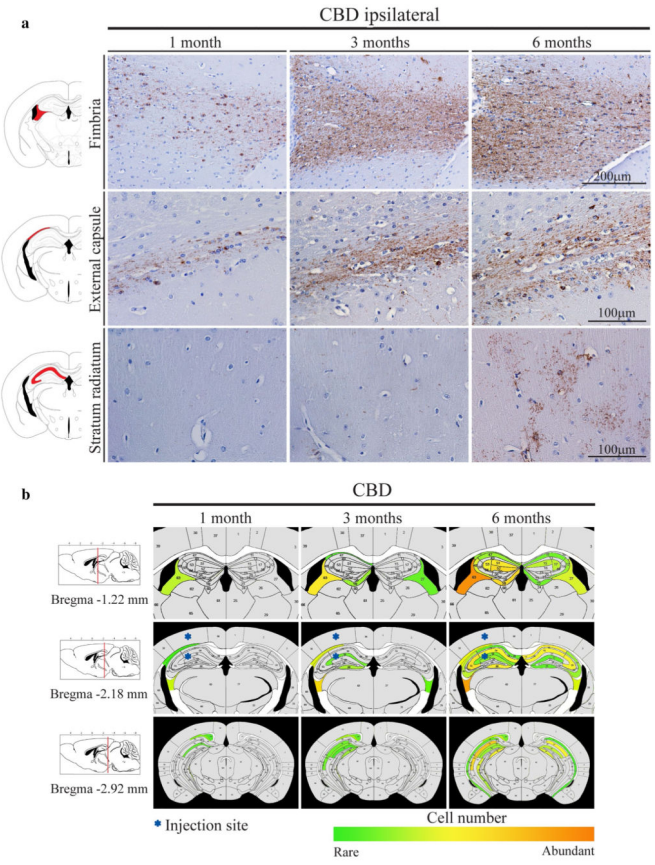

Fig. 3.

Tau inclusions that developed in PS19 mice injected with CBD-Tau increased in intensity and spread to regions distal from the injection site with increasing post-injection survival times. **a** Microphotographs of brain sections immunostained with AT8 showing the fimbria, alveus/external capsule and stratum radiatum ipsilateral to the injection site in the PS19 mice at 1, 3, 6 months post-injection. *Scale bar*, *upper row* 200 μm; *middle* and *lower rows* 100 μm. **b** Heatmaps of coronal sections showing the CBD-Tau-induced glial tau pathology at the same time points as in (**a**). Quantification [1 month (n = 6), 3 months (n = 6) and 6 months (n = 6)] was conducted as described in “Materials and methods” to generate these heatmaps. Each heatmap *panel* represents pathology distribution in one of the three coronal planes (Bregma −1.22, −2.18 and −2.92). *Left column* shows sagittal view of the selected coronal planes indicated by a *red line*. *Blue stars* indicate injection site

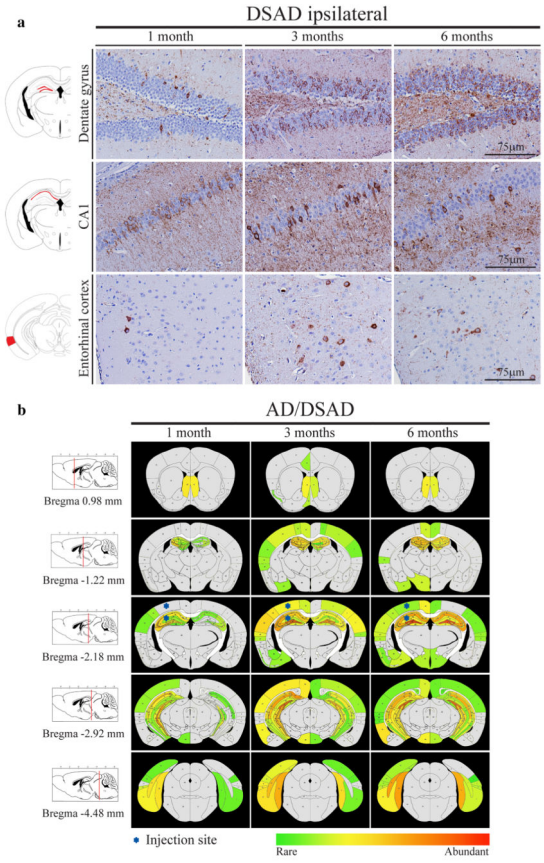

Fig. 4.

Neuronal tau inclusions developed in PS19 mice injected with AD-Tau and DSAD-Tau and they increased in abundance, intensity and spread to regions distal from the injected site with increasing post-injection survival times. **a** Microscopic images of brain sections of DSAD-Tau-injected mice. The images are representative of the dentate gyrus, CA1 and entorhinal cortex of the side ipsilateral to the injection following IHC with AT8 at 1, 3, 6 months post-injection. *Scale bars* 75 μm. **b** Heatmaps of coronal sections of tau pathology seen after injection at the same time points as in (**a**). Semiquantitative analysis of AT8 pathology was performed in AD-Tau- and DSAD-Tau-injected mice and combined in the heatmap here [1 month (n = 8), 3 months (n = 8) and 6 months (n = 8)]. Each *panel* represents pathology distribution in one of the five coronal planes (Bregma 0.98, −1.22 −2.18, −2.92 and −4.48 mm) at different time points after injection. *Left column* shows sagittal view of the selected coronal planes that are indicated by a *red line*. *Blue stars* indicate injection site

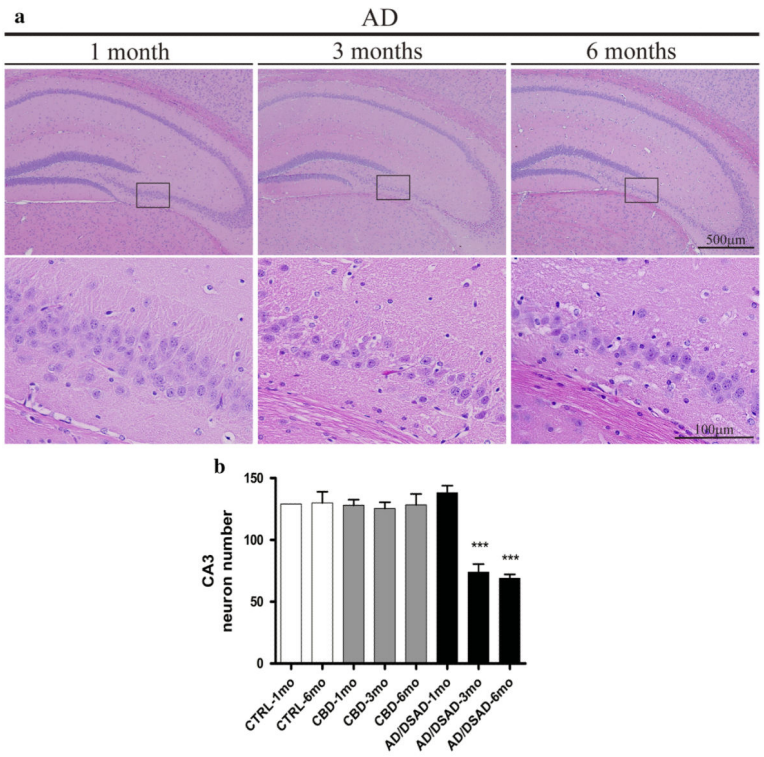

Fig. 5.

There is neuron loss in the CA3 region of PS19 mice injected with AD-Tau and DSAD-Tau at 3 and 6 months post-injection. **a** The *upper row* of images show H&E stained low-power microphotographs of the hippocampus contralateral to the AD-Tau injection in PS19 mice at 1, 3, and 6 months post-injection. The microphotographs in the *lower row* show higher magnification images of the *boxed areas* in the *upper row*. *Scale bar*, *upper row* 500 μm; *lower row* 100 μm. **b** Quantification of the neurons in the CA3 region of PS19 mice injected with non-pathological or control (CTRL-Tau) human brain extract versus enriched CBD-Tau or AD-Tau and DSAD-Tau fractions. *Error bars* indicate SEM; ***$p < 0.001$, as determined by one-way ANOVA and Tukey's multiple-comparison test, with $n = 2$ in CTRL-Tau at 1 month and 6 months; $n = 5$ in CBD-Tau at 1 month and 3 months; $n = 6$ in CBD-Tau at 6 months; and $n = 7$ in AD/DSAD-Tau at 1, 3 and 6 months

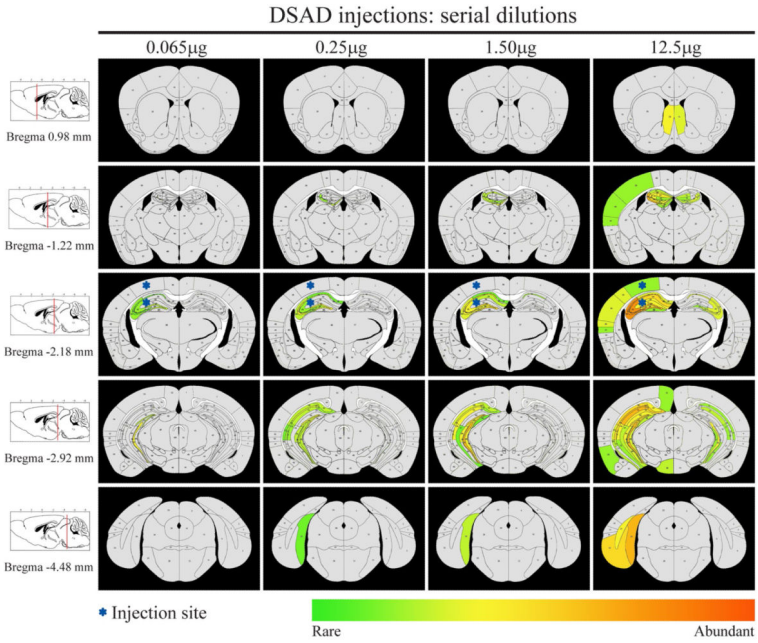

Fig. 6.

Dose-dependent increase in tau pathology in PS19 mice after the injection of human brain derived DSAD-Tau. At 1 month after injection, the burden of tau pathology increases and the distribution of pathology is more extensive throughout brain structures following injections of increasing amounts of injected pathological tau. Heatmaps of coronal sections of tau pathology after injections of serial dilutions of DSAD-Tau into PS19 mice. Each *panel* represents pathology distribution in one of the five coronal planes (Bregma 0.98, −1.22 −2.18, −2.92 and −4.48 mm) at 1 month post-injection (n = 3 for each dose of DSAD-Tau). *Left column* shows sagittal view of the selected coronal planes that are indicated by a *red line*. *Blue stars* indicate injection site

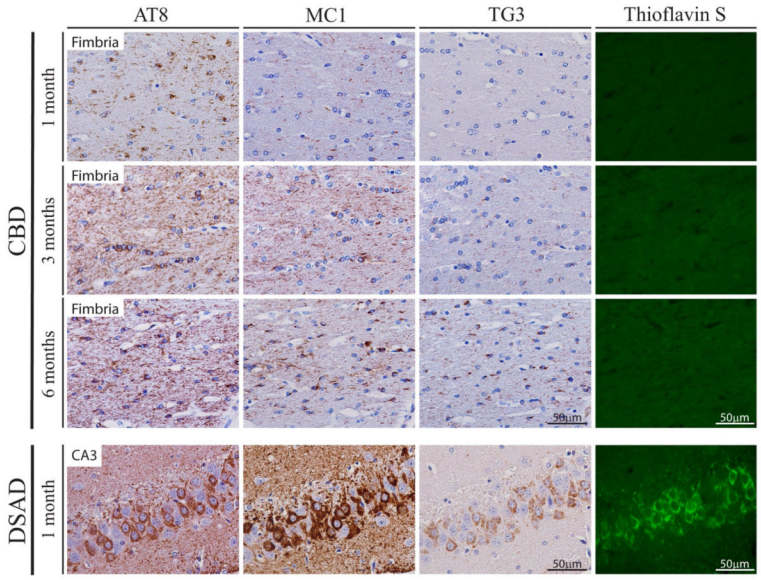

Fig. 7.

Tau inclusions in PS19 mice after injection of CBD-Tau and DSAD-Tau show properties that recapitulate their human disease counterparts. Microphotographs are of brain sections stained with mAbs AT8, MC1 and TG3 to detect abnormal phosphorylation (AT8) and conformational (MC1, TG3) changes in pathological tau and ThS histochemistry to demonstrate the amyloid properties of the inclusions. Shown here are the fimbria of Tg mice injected with CBD-Tau at 1 month, 3 and 6 months post-injection (*upper three rows*) and CA3 of Tg mice injected with DSAD-Tau extracts at 1 month after injection (*lower row*). *Scale bars* 50 μm

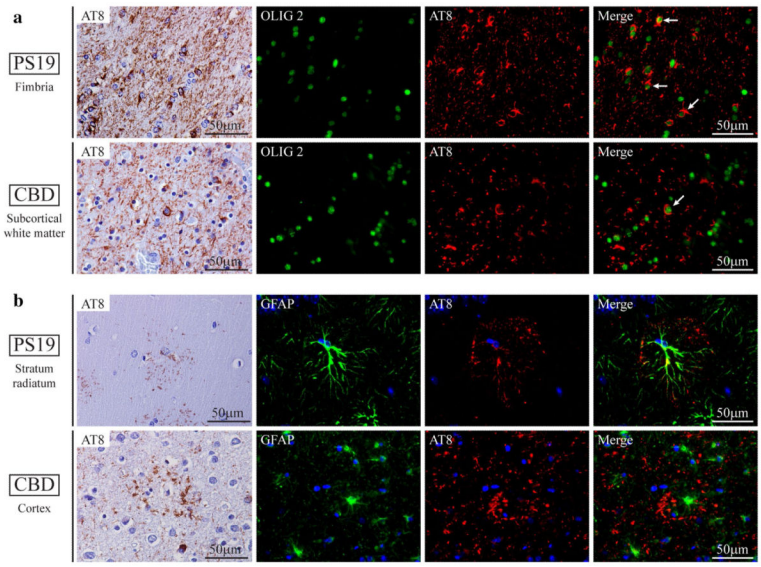

Fig. 8.

Accumulation of tau pathology in oligodendrocytes and astrocytes in PS19 mice injected with CBD-Tau parallels pathology of sporadic CBD in humans. **a** Brain sections stained with mAb AT8 in the far *left column*, while the 3 columns to the *right* show double immunofluorescence with Olig2 (*green* in nucleus), AT8 (*red* in cytoplasm and neurites) and merged images in the fimbria of a PS19 mouse 6 months after injection (*upper row*) and subcortical white matter of the cingulate gyrus in a sporadic CBD case (*lower row*). **b** Brain sections stained with mAb AT8 and double immunofluorescence with GFAP (*green*), AT8 (*red*) and merged images in the stratum radiatum of the hippocampus of a PS19 mouse 6 months after injection (*upper row*) and gray matter of the parietal cortex of a sporadic CBD case (lower row). *Scale bar* 50 μm

Table 1

PS19 mice used for the experiments

Injections of CBD-Tau and CTRL-Tau				
CBD (*n* = 18 mice)				
Time postinjection (months)	Number of mice		Total injected tau (μg)	
	CBD-1	CBD-2		
1	4	2	0.05	
3	4	2	0.05	
6	4	2	0.05	
CTRL (*n* = 4 mice)				
Time postinjection (months)	Number of mice	Total injected tau (μg)		
1	2	0.003		
6	2	0.003		
Injections of AD-Tau and DSAD-Tau				
AD (*n* = 12 mice)/*DSAD* (*n* = 12 mice)				
Time postinjection (months)	Number of mice		Total injected tau (μg)	
	AD	DSAD	AD	DSAD
1	4	4	10.5	12.5
3	4	4	10.5	12.5
6	4	4	10.5	12.5
DSAD serial dilutions (*n* = 12 mice)				
Time postinjection (months)	Number of mice	Total injected tau (μg)		
1	3	0.065		
1	3	0.25		
1	3	1.5		
1	3	12.5		

All mice were injected at two sites: right hippocampus and overlying cortex. The injected volume for all mice was 5 μl total (2.5 μl/site). CBD1 and CBD2 represent CBD-Tau generated from two different CBD brains. All mice were 2 months old at time of injection except for the group injected with CBD-Tau (CBD-1) that were 5 months old at time of injection. The older mice did not show any differences in the distribution and extent of tau pathology since mice injected with CBD-Tau from CBD1 and CBD2 brains were similar